Perfect Tracking Control of Dual-Input Dual-Output System for High-Precision Stage in Translation and Pitching Motion

Masahiro Mae*a) Student Member, Wataru Ohnishi* Student Member
Hiroshi Fujimoto* Senior Member, Yoichi Hori* Fellow

High-precision stages are widely used for manufacturing semiconductors and flat panels. These high-precision stages have become multi-input multi-output (MIMO) systems with 6 degrees of freedom (DOF), and hence, the coupling between the translation and pitching motion deteriorates the control performance. This paper proposes the multirate feedforward control for MIMO system and applies to these high-precision stages. The multirate feedforward control designs the stable inversion for the unstable discretization zero problem. In addition, the design of the MIMO multirate feedforward controllers has a degree of freedom to make the $\boldsymbol{B}$ matrix according to the selection of generalized controllability indices. In conventional control methods such as precompensated decoupling controllers, it is theoretically impossible to achieve perfect tracking because the unstable discretization zeros are generated. In this paper, the proposed method is applied to translation and pitching motion of a high-precision stage, and it achieves perfect tracking in the simulation. The effectiveness of the proposed method is verified by experiments.

Keywords: multirate feedforward, multi-imput multi-output system, high-precision stage

1. Introduction

A high-precision scan stage plays an important role in manufacturing semiconductors and flat panels [(1)]. The circuit configuration of semiconductors and flat panels becomes finer exponentially year by year [(2)]. The conventional high-precision stage is a 1 degree of freedom (DOF) system mechanically constrained to move only one direction. Recently, in order to decrease the disturbance of vibration from the floor and friction from the mechanical restraint, the high-precision stage is 6 DOF ($x, y, z, \theta_x, \theta_y, \theta_z$) system by the gravity canceller which compensates for the gravitational force experienced by the fine stage [(1)]. In the stage with 6 DOF, the interference forces between the axes worsen the positioning accuracy of the stage. Many kinds of research have been conducted on the decoupling by precompensator [(1)] and the integrating design of mechanical systems and control methods [(3)]. In the proposed method, perfect tracking control (PTC) is achieved by considering the interference between axes by using multi-input multi-output (MIMO) multirate feedforward controller. The word "perfect tracking control (PTC)" is defined as "the plant output perfectly tracks the desired trajectory with zero tracking error at every sampling point" [(4)]. As a result, the proposed MIMO multirate feedforward controller relaxes the limitations of the mechanical design which exists to suppress the interference force.

In this paper, the authors control a high-precision stage with 6 DOF as shown in Fig. 1(a). The authors consider about 2 DOF of translation in the x axis direction and pitching around the y axis as shown in Fig. 1(b). The effectiveness of the proposed method is demonstrated by the simulation and the experiment.

a) Correspondence to: mae.masahiro17@ae.k.u-tokyo.ac.jp
* The University of Tokyo
5-1-5, Kashiwanoha, Kashiwa, Chiba, 227-8561 Japan
Phone: +81-4-7136-3881
Fax: +81-4-7136-3881

2. Proposed Method

2.1 Multirate Feedforward for Single-Input Single-Output System

Multirate feedforward control achieves PTC [(6)]. A digital tracking control system usually has two samplers for the reference signal $r(t)$ and the output $y(t)$, and one holder on the input $u(t)$, as shown in Fig. 2. Therefore, there exist three time periods T_r, T_y, and T_u which represent the periods of $r(t)$, $y(t)$, and $u(t)$, respectively, as shown in Fig. 3. Additionally, the longer period of T_r and T_y is defined as the frame period T_f. In the case of the single-input single-output (SISO) nth-order plant, $T_r = nT_y = nT_u = T_f$.

Consider the continuous-time nth-order plant described by the state equation (1) and the output equation (2).

$$\dot{\boldsymbol{x}}(t) = \boldsymbol{A}_c\boldsymbol{x}(t) + \boldsymbol{b}_c\boldsymbol{u}(t) \cdots (1)$$
$$y(t) = \boldsymbol{c}_c\boldsymbol{x}(t) \cdots (2)$$

From discretization of (1) and (2) by zero order hold in sampling period T_u, the discrete-time plant becomes the state equation (3) and output equation (4).

$$\boldsymbol{x}[k+1] = \boldsymbol{A}_s\boldsymbol{x}[k] + \boldsymbol{b}_s u[k] \cdots (3)$$
$$y[k] = \boldsymbol{c}_s\boldsymbol{x}[k] \cdots (4)$$

where the matrices $\boldsymbol{A}_s$, $\boldsymbol{b}_s$, and $\boldsymbol{c}_s$ are given by

$$\boldsymbol{A}_s = e^{\boldsymbol{A}_c T_u}, \cdots (5)$$
$$\boldsymbol{b}_s = \int_0^{T_u} e^{\boldsymbol{A}_c \tau}\boldsymbol{b}_c d\tau, \cdots (6)$$

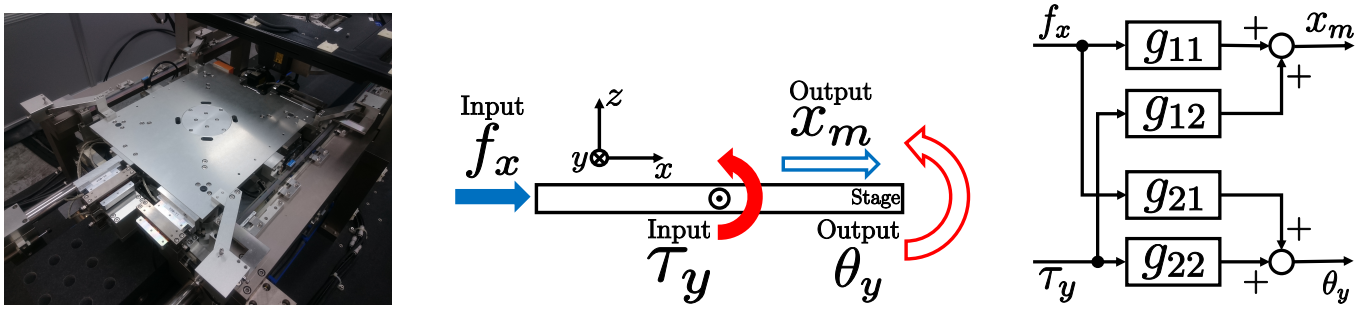

(a) Photograph of the 6-DOF high-precision stage. (b) Interference between x and θ_y. (c) Block diagram of the plant.

Fig. 1. Details of the plant.

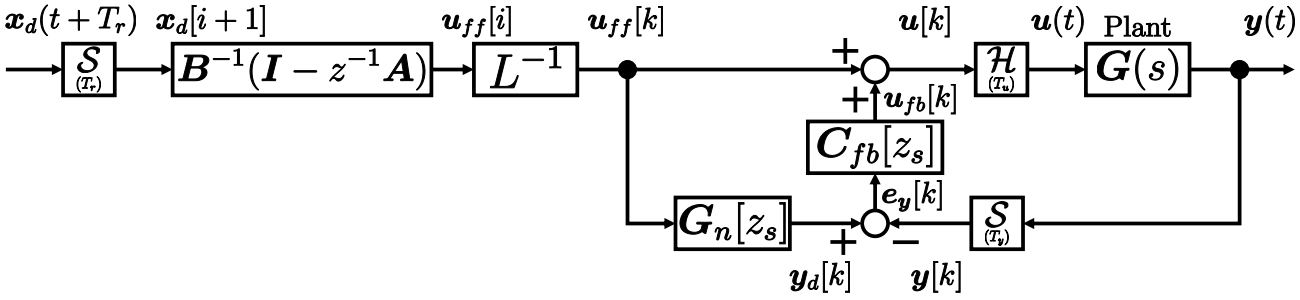

Fig. 2. Block diagram of the controller with the plant which does not have unstable intrinsic zeros. $\mathcal{S}$, $\mathcal{H}$, and L denote a sampler, holder, and lifting operator [5], respectively, z and z_s denote e^{sT_r} and e^{sT_u}, respectively.

$$\boldsymbol{c}_s = \boldsymbol{c}_c. \quad \cdots (7)$$

By lifting the discrete-time state equation (3) and the output equation (4), the state equation (8) and the output equation (9) are given by

$$\boldsymbol{x}[i+1] = \boldsymbol{A}\boldsymbol{x}[i] + \boldsymbol{B}\boldsymbol{u}[i], \quad \cdots (8)$$
$$y[i] = \boldsymbol{c}\boldsymbol{x}[i], \quad \cdots (9)$$

where the matrices $\boldsymbol{A}$, $\boldsymbol{B}$, and $\boldsymbol{c}$, and i are given by

$$\boldsymbol{A} = \boldsymbol{A}_s^n, \quad \cdots (10)$$
$$\boldsymbol{B} = \begin{bmatrix} \boldsymbol{A}_s^{n-1}\boldsymbol{b}_s & \boldsymbol{A}_s^{n-2}\boldsymbol{b}_s & \cdots & \boldsymbol{A}_s\boldsymbol{b}_s & \boldsymbol{b}_s \end{bmatrix}, \quad \cdots (11)$$
$$\boldsymbol{c} = \boldsymbol{c}_s, \quad \cdots (12)$$
$$\boldsymbol{x}[i] = \boldsymbol{x}(iT_r). \quad \cdots (13)$$

Equation (8) and (9) are given from the interval between $t = iT_r = kT_u$ and $t = (i+1)T_r = (k+n)T_u$. Input and output vectors $\boldsymbol{u}[i]$ (14) and $\boldsymbol{y}[i]$ (15) are given by

$$\begin{aligned} \boldsymbol{u}[i] &= \begin{bmatrix} u_1[i] & u_2[i] & \cdots & u_n[i] \end{bmatrix}^T \\ &= \begin{bmatrix} u(kT_u) & u((k+1)T_u) & \cdots & u((k+n-1)T_u) \end{bmatrix}^T, \end{aligned} \quad \cdots (14)$$

$$\begin{aligned} \boldsymbol{y}[i] &= \begin{bmatrix} y_1[i] & y_2[i] & \cdots & y_n[i] \end{bmatrix}^T \\ &= \begin{bmatrix} y(kT_y) & y((k+1)T_y) & \cdots & y((k+n-1)T_y) \end{bmatrix}^T. \end{aligned} \quad \cdots (15)$$

From (8), the control input $\boldsymbol{u}_{ff}[i]$ to achieve PTC are given by

$$\boldsymbol{u}_{ff}[i] = \boldsymbol{B}^{-1}(\boldsymbol{I} - z^{-1}\boldsymbol{A})\boldsymbol{x}[i+1]. \quad \cdots (16)$$

The block diagram of the control system is shown in Fig. 2. L is a discrete-time lifting operator [5]. L^{-1} outputs the elements of nth dimensional vector $\boldsymbol{u}_{ff}[i]$, which is input every period T_r, in order from 1 to n by $T_u = T_r/n$.

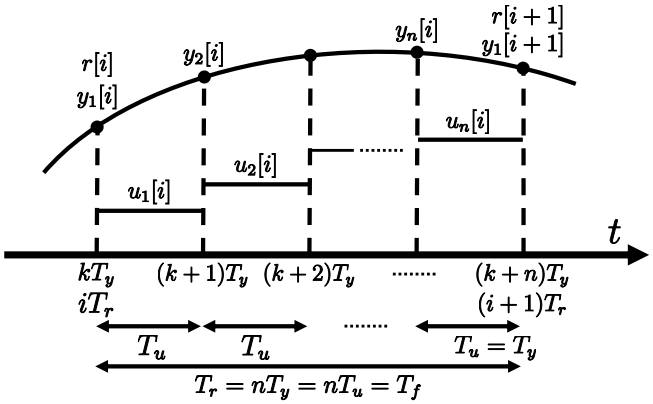

Fig. 3. Multirate sampling control at same interval.

2.2 Multirate Feedforward for MIMO System

In m-input p-output nth order MIMO system, the state equation (17) and the output equation (18) of the continuous-time plant are given by

$$\dot{\boldsymbol{x}}(t) = \boldsymbol{A}_c\boldsymbol{x}(t) + \boldsymbol{B}_c\boldsymbol{u}(t) \quad \cdots (17)$$
$$\boldsymbol{y}(t) = \boldsymbol{C}_c\boldsymbol{x}(t) \quad \cdots (18)$$
$$\boldsymbol{B}_c = \begin{bmatrix} \boldsymbol{b}_{c1} & \cdots & \boldsymbol{b}_{cm} \end{bmatrix} \quad \cdots (19)$$
$$\boldsymbol{C}_c = \begin{bmatrix} \boldsymbol{c}_{c1} & \cdots & \boldsymbol{c}_{cp} \end{bmatrix}^T \quad \cdots (20)$$

where the plant state $\boldsymbol{x} \in \mathbb{R}^n$, the plant input $\boldsymbol{u} \in \mathbb{R}^m$, and the plant output $\boldsymbol{u} \in \mathbb{R}^p$.

Generalized controllability indices are defined as follows [7].

Definition (Generalized Controllability Indices)**.** *Generalized controllability indices of* $(\boldsymbol{A}_c, \boldsymbol{B}_c)$ *are defined as follows for* $\boldsymbol{A}_c \in \mathbb{R}^{n\times n}$ *and* $\boldsymbol{B}_c = [\boldsymbol{b}_{c1}, \cdots, \boldsymbol{b}_{cm}] \in \mathbb{R}^{n\times m}$*. If* $(\boldsymbol{A}_c, \boldsymbol{B}_c)$ *is a controllable pair, n linearly independent vectors can be*

selected from
$\{\boldsymbol{b}_{c1}, \cdots, \boldsymbol{b}_{cm}, \boldsymbol{A}_c\boldsymbol{b}_{c1}, \cdots, \boldsymbol{A}_c\boldsymbol{b}_{cm}, \cdots, \boldsymbol{A}_c^{n-1}\boldsymbol{b}_{cm}\}$.

Letting φ be a set of these n vectors, σ_l, and N are defined by

$$\sigma_l = \text{number}\{k|\boldsymbol{A}_c^{k-1}\boldsymbol{b}_{cl} \in \varphi\}, \cdots\cdots\cdots\cdots (21)$$

$$\sum_{l=1}^{m} \sigma_l = n, \cdots\cdots\cdots\cdots\cdots\cdots\cdots\cdots (22)$$

$$N = \max(\sigma_l). \cdots\cdots\cdots\cdots\cdots\cdots\cdots\cdots (23)$$

In the case of MIMO system, n (= plant order) number of vectors are selected from generalized controllability indices, and the full row rank matrix $\boldsymbol{B}$ are designed. Therefore, the feedforward controllers designed according to their choice have different forms.

From (24), the control input $\boldsymbol{u}_{ff}[i]$ to achieve PTC are given by (25).

$$\boldsymbol{x}[i+1] = \boldsymbol{A}\boldsymbol{x}[i] + \boldsymbol{B}\boldsymbol{u}[i], \cdots\cdots\cdots\cdots\cdots\cdots (24)$$

$$\boldsymbol{u}_{ff}[i] = \boldsymbol{B}^{-1}(\boldsymbol{I} - z^{-1}\boldsymbol{A})\boldsymbol{x}[i+1], \cdots\cdots\cdots\cdots (25)$$

where the matrices $\boldsymbol{A}$, $\boldsymbol{x}[i]$, $\boldsymbol{u}[i]$, and z are given by

$$\boldsymbol{A} = e^{\boldsymbol{A}_c T_f}, \cdots\cdots\cdots\cdots\cdots\cdots\cdots\cdots (26)$$

$$\boldsymbol{x}[i] = \boldsymbol{x}(iT_f), \cdots\cdots\cdots\cdots\cdots\cdots\cdots\cdots (27)$$

$$\boldsymbol{u}[i] = \begin{bmatrix}\boldsymbol{u}_1[i] & \cdots & \boldsymbol{u}_m[i]\end{bmatrix}^T = \begin{bmatrix}u_{11}[i], & \cdots, & u_{1N_1}, & u_{21}[i], & \cdots, & u_{mN_m}[i]\end{bmatrix}^T, \cdots\cdots\cdots\cdots\cdots\cdots\cdots\cdots (28)$$

$$z = e^{sT_f}, \cdots\cdots\cdots\cdots\cdots\cdots\cdots\cdots (29)$$

$$T_f = NT_u. \cdots\cdots\cdots\cdots\cdots\cdots\cdots\cdots (30)$$

where the input multiplicity of N_l ($l = 1, 2, \cdots, m$) is chosen so that the matrix $\boldsymbol{B}$ is full row rank and fulfills (31).

$$N_l \geq \sigma_l \cdots\cdots\cdots\cdots\cdots\cdots\cdots\cdots (31)$$

3. Modeling

In the simulation and experiment, the authors control the fine stage of the 6 DOF high-precision stage shown in Fig. 1(a). This fine stage is supported by 6 DOF air bearing gravity canceller. In this paper, controlling 2 DOF of the translation x along the x axis and the pitching θ_y around and y axis, as shown in Fig. 1(b).

3.1 System Identification The equations of motion of the translation and pitching of the stage are given by (32) and (33) [8].

$$(M_{x1} + M_{x2})\ddot{x}_{g1} + C_{x1}\dot{x}_{g1} + K_{x1}x_{g1} + M_{x2}L_{g2}\ddot{\theta}_y = f_x \cdots\cdots (32)$$

$$(M_{x2}L_{g2}^2 + J_{\theta y})\ddot{\theta}_y + C_{\theta y}\dot{\theta}_y + K_{\theta y}\theta_y + M_{x2}L_{g2}(\ddot{x}_{g1} - g\theta_y) = \tau_y + f_x L_{fx} \cdots (33)$$

Convert x_{g1} to observable x_m by (34).

$$x_m(s) = x_{g1}(s) + L_m\theta_y(s) \cdots\cdots\cdots\cdots\cdots\cdots (34)$$

From the expressions (32), (33), and (34), transfer functions g_{11} to g_{22} are given by (35) to (38).

A parameters of the stage are shown in Table 1, which is given from fitting in the frequency domain, shown in Fig. 6.

Table 1. Model parameters.

Symbol	Meaning	Value
x_m	Measured position of the fine stage	–
x_{g1}	Position of the CoG of the planar air bearing and the air gyro	–
x_{g2}	Position of the CoG of the fine stage	–
θ_y	Measured attitude angle of the fine stage	–
f_x	Input force of the fine stage in the x direction	–
τ_y	Input torque of the fine stage in the θ_y direction	–
M_{x1}	Mass of the planar air bearing and the air gyro	0.077 kg
C_{x1}	Viscosity coefficient in the x_{g1} motion	300 N/(m/s)
K_{x1}	Spring coefficient in the x_{g1} motion	6000 N/m
M_{x2}	Mass of the fine stage	5.3 kg
$J_{\theta y}$	Moment of inertia of the fine stage	0.10 kgm^2
$C_{\theta y}$	Viscosity coefficient of the fine stage in the θ_y motion	1.6 Nm/(rad/s)
$K_{\theta y}$	Spring coefficient of the fine stage in the θ_y motion	1200 Nm/rad
L_m	Distance between the measurement point of x_m and the CoR	−0.028 m
L_{g2}	Distance between the CoR and the CoG of the fine stage	−0.051 m
L_{fx}	Distance between the CoR of the fine stage and the actuation point	−0.0026 m

3.2 State Space Realization a_{ij}, b_{ik} ($i \in \{2, 4\}$, $j \in \{1, 2, 3, 4\}$, $k \in \{1, 2\}$) from the expressions (32), (33), and (34), $(\ddot{x}_m, \ddot{\theta}_y)$ explained by $(x_m, \dot{x}_m, \theta_y, \dot{\theta}_y)$ are given by (40) and (41).

$$\ddot{x}_m = a_{21}x_m + a_{22}\dot{x}_m + a_{23}\theta_y + a_{24}\dot{\theta}_y + b_{21}f_x + b_{22}\tau_y \cdots (40)$$

$$\ddot{\theta}_y = a_{41}x_m + a_{42}\dot{x}_m + a_{43}\theta_y + a_{44}\dot{\theta}_y + b_{41}f_x + b_{42}\tau_y \cdots (41)$$

(40) and (41) can be expressed in the form of (42) and (43).

$$\begin{bmatrix}\dot{x}_m \\ \ddot{x}_m \\ \dot{\theta}_y \\ \ddot{\theta}_y\end{bmatrix} = \begin{bmatrix}0 & 1 & 0 & 0 \\ a_{21} & a_{22} & a_{23} & a_{24} \\ 0 & 0 & 0 & 1 \\ a_{41} & a_{42} & a_{43} & a_{44}\end{bmatrix}\begin{bmatrix}x_m \\ \dot{x}_m \\ \theta_y \\ \dot{\theta}_y\end{bmatrix} + \begin{bmatrix}0 & 0 \\ b_{21} & b_{22} \\ 0 & 0 \\ b_{41} & b_{42}\end{bmatrix}\begin{bmatrix}f_x \\ \tau_y\end{bmatrix} \cdots (42)$$

$$\begin{bmatrix}x_m \\ \theta_y\end{bmatrix} = \begin{bmatrix}1 & 0 & 0 & 0 \\ 0 & 0 & 1 & 0\end{bmatrix}\begin{bmatrix}x_m \\ \dot{x}_m \\ \theta_y \\ \dot{\theta}_y\end{bmatrix} \cdots\cdots\cdots\cdots (43)$$

The state equations (44) and output equations (45) of the continuous-time plant are given by

$$\dot{\boldsymbol{x}}(t) = \boldsymbol{A}_c\boldsymbol{x}(t) + \boldsymbol{B}_c\boldsymbol{u}(t), \cdots\cdots\cdots\cdots\cdots\cdots (44)$$

$$\boldsymbol{y}(t) = \boldsymbol{C}_c\boldsymbol{x}(t), \cdots\cdots\cdots\cdots\cdots\cdots\cdots\cdots (45)$$

where the vectors $\boldsymbol{x}(t)$, $\boldsymbol{u}(t)$, and $\boldsymbol{y}(t)$, and the matrices $\boldsymbol{A}_c$, $\boldsymbol{B}_c$, and $\boldsymbol{C}_c$ are given by

$$\boldsymbol{x}(t) = \begin{bmatrix}x_m \\ \dot{x}_m \\ \theta_y \\ \dot{\theta}_y\end{bmatrix}, \qquad \boldsymbol{u}(t) = \begin{bmatrix}f_x \\ \tau_y\end{bmatrix}, \qquad \boldsymbol{y}(t) = \begin{bmatrix}x_m \\ \theta_y\end{bmatrix},$$

$$\boldsymbol{A}_c = \begin{bmatrix}0 & 1 & 0 & 0 \\ a_{21} & a_{22} & a_{23} & a_{24} \\ 0 & 0 & 0 & 1 \\ a_{41} & a_{42} & a_{43} & a_{44}\end{bmatrix},$$

$$\boldsymbol{B}_c = \begin{bmatrix}0 & 0 \\ b_{21} & b_{22} \\ 0 & 0 \\ b_{41} & b_{42}\end{bmatrix} = \begin{bmatrix}\boldsymbol{b}_{c1} & \boldsymbol{b}_{c2}\end{bmatrix},$$

$$\boldsymbol{C}_c = \begin{bmatrix}1 & 0 & 0 & 0 \\ 0 & 0 & 1 & 0\end{bmatrix}.$$

By using zero order hold to the state state equation (44) and the output equation (45) of the continuous-time plant with the sampling period T_u, the state equation (46) and the output

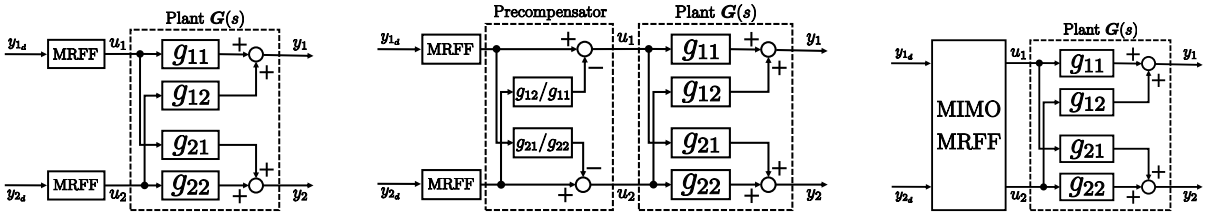

(a) Conventional method 1. (b) Conventional method 2. (c) Proposed method.

Fig. 4. Block diagram of the control methods. These show only feedforward controllers.

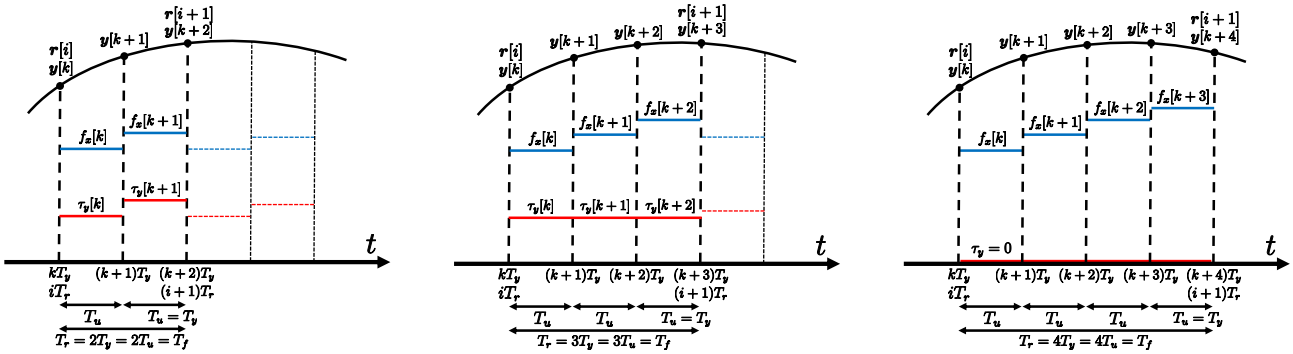

(a) $(\sigma_1, \sigma_2) = (2, 2)$ (b) $(\sigma_1, \sigma_2) = (3, 1)$ (c) $(\sigma_1, \sigma_2) = (4, 0)$

Fig. 5. MIMO multirate input control.

$$g_{11}(s) = \frac{x_m(s)}{f_x(s)} = \frac{[J_{\theta y} + L_{fx}L_m M_{x1} - (L_{fx} - L_{g2})(L_{g2} - L_m)M_{x2}]s^2 + (C_{\theta y} + L_{fx}L_m C_{x1})s + L_{fx}L_m K_{x1} - L_{g2}M_{x2}g}{D(s)} \quad (35)$$

$$g_{12}(s) = \frac{x_m(s)}{\tau_y(s)} = \frac{[L_m M_{x1} + (L_m - L_{g2})M_{x2}]s^2 + L_m C_{x1}s + L_m K_{x1}}{D(s)} \quad (36)$$

$$g_{21}(s) = \frac{\theta_y(s)}{f_x(s)} = \frac{[L_{fx}M_{x1} + (L_{fx} - L_{g2})M_{x2}]s^2 + L_{fx}C_{x1}s + L_{fx}K_{x1}}{D(s)} \quad (37)$$

$$g_{22}(s) = \frac{\theta_y(s)}{\tau_y(s)} = \frac{(M_{x1} + M_{x2})s^2 + C_{x1}s + K_{x1}}{D(s)} \quad (38)$$

$$D(s) = [(M_{x1} + M_{x2})J_{\theta y} + M_{x1}M_{x2}L_{g2}^2]s^4 + [(M_{x1} + M_{x2})C_{\theta y} + (J_{\theta y} + M_{x2}L_{g2}^2)C_{x1}]s^3 + [(J_{\theta y} + M_{x2}L_{g2}^2)K_{x1} + (M_{x1} + M_{x2})(K_{\theta y} - M_{x2}L_{g2}g) + C_{\theta y}C_{x1}]s^2$$
$$+ [C_{\theta y}K_{x1} + C_{x1}(K_{\theta y} - L_{g2}M_{x2}g)]s + K_{x1}(K_{\theta y} - L_{g2}M_{x2}g) \quad (39)$$

equation (47) of the discrete-time plant are given by

$$\boldsymbol{x}[k+1] = \boldsymbol{A}_s\boldsymbol{x}[k] + \boldsymbol{B}_s\boldsymbol{u}[k], \quad (46)$$
$$\boldsymbol{y}[k] = \boldsymbol{C}_s\boldsymbol{x}[k], \quad (47)$$

where $\boldsymbol{x}[k]$, $\boldsymbol{u}[k]$, $\boldsymbol{y}[k]$, and $\boldsymbol{B}_s$ are given by

$$\boldsymbol{x}[k] = \begin{bmatrix} x_m[k] \\ \dot{x}_m[k] \\ \theta_y[k] \\ \dot{\theta}_y[k] \end{bmatrix}, \qquad \boldsymbol{u}[k] = \begin{bmatrix} f_x[k] \\ \tau_y[k] \end{bmatrix}, \qquad \boldsymbol{y}[k] = \begin{bmatrix} x_m[k] \\ \theta_y[k] \end{bmatrix},$$

$$\boldsymbol{B}_s = \begin{bmatrix} \boldsymbol{b}_{s1} & \boldsymbol{b}_{s2} \end{bmatrix}.$$

When constructing the square matrix $\boldsymbol{B}$, generalized controllability indices are given by

$$\{\boldsymbol{b}_{s1}, \boldsymbol{b}_{s2}, \boldsymbol{A}_s\boldsymbol{b}_{s1}, \boldsymbol{A}_s\boldsymbol{b}_{s2}, \boldsymbol{A}_s^2\boldsymbol{b}_{s1}, \boldsymbol{A}_s^2\boldsymbol{b}_{s2}, \boldsymbol{A}_s^3\boldsymbol{b}_{s1}, \boldsymbol{A}_s^3\boldsymbol{b}_{s2}\}.$$

When the plant order is $n = 4$, 4 elements are chosen from generalized controllability indices to constract the square matrix $\boldsymbol{B}$.

4. Experiment

4.1 Condition The block diagram of the simulation is shown in Fig. 2.

Generally, a dual-input dual-output plant with the interference is represented by a block diagram as shown in Fig. 1(c). g_{11} to g_{22} represent the transfer function of each path.

Conventional method 1 ignores the interference by g_{12} and g_{21} and the multirate feedforward controllers are designed for each SISO system g_{11} and g_{22}, respectively, as shown in Fig. 4(a). Coupling is suppressed by the feedback controller.

Conventional method 2 designs a precompensator for continuous-time plants that cancels the interference between axes by g_{12} and g_{21}, and the multirate feedforward controllers are designed for each decoupled SISO system g_{11} and g_{22}, respectively, as shown in Fig. 4(b). In this method, the precompensator is discretized by the bilinear transformation. Since the problem of the unstable discretization zero is not considered, PTC cannot theoretically be achieved.

In the proposed method, a dual-input dual-output multirate feedforward controller is designed for a dual-input dual-output plant as shown in Fig. 4(c).

In Fig. 6, $\boldsymbol{G}_4$ is used for MIMO plant model of the proposed method, and $\boldsymbol{G}_2$ is used for SISO plant model of the conventional method 1 and 2.

In the simulation, $\boldsymbol{C}_{fb}[z_s]$, which is the feedback controller,

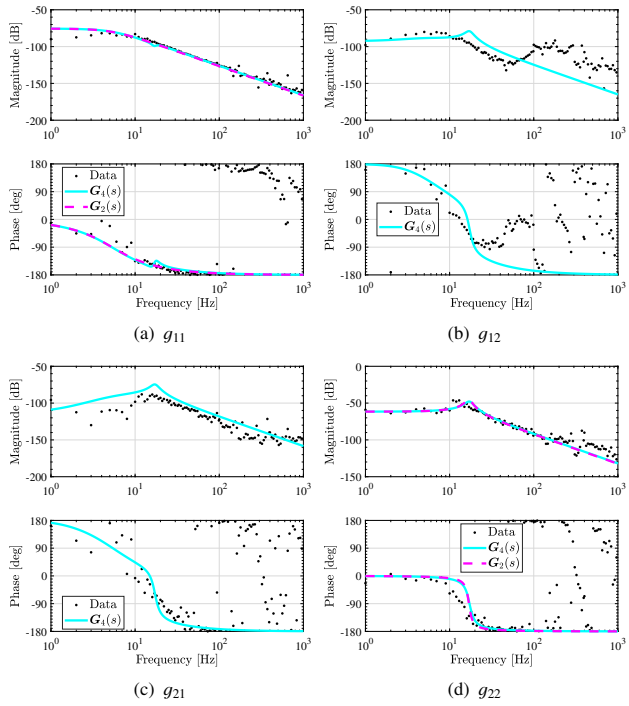

(a) g_{11} (b) g_{12}

(c) g_{21} (d) g_{22}

Fig. 6. Frequency responses of the plant. $\boldsymbol{G}_4$ and $\boldsymbol{G}_2$ denote a 4th order MIMO nominal plant and a 2nd order SISO nominal plant, respectively.

is 0 in the all methods. In the experiment, $\boldsymbol{C}_{fb}[z_s]$ is PID controllers tuned to have 20 Hz closed roop pole for all 6 DOF $(x, y, z, \theta_x, \theta_y, \theta_z)$ in the all methods.

7th-order polynomial trajectory of $0 \sim 100\,\mu$m in $0 \sim 20$ ms is given for x_m^{ref} and a zero constant reference is given for θ_y^{ref}. $T_u = 200\,\mu$s, $N = \max(\sigma_1, \sigma_2)$, and $T_r = T_y = NT_u = T_f$.

4.2 Simulation Result In this paper, the simulation of the proposed method, which has three ways of selecting generalized controllability indices as shown in Fig. 5, is conducted with the conventional method.

$$(\sigma_1, \sigma_2) = (2, 2)$$
$$\Rightarrow \boldsymbol{B} = \begin{bmatrix} \boldsymbol{A}_s\boldsymbol{b}_{s1} & \boldsymbol{b}_{s1} & \boldsymbol{A}_s\boldsymbol{b}_{s2} & \boldsymbol{b}_{s2} \end{bmatrix} \cdots\cdots\cdots\cdots\cdots (48)$$
$$(\sigma_1, \sigma_2) = (3, 1)$$
$$\Rightarrow \boldsymbol{B} = \begin{bmatrix} \boldsymbol{A}_s^2\boldsymbol{b}_{s1} & \boldsymbol{A}_s\boldsymbol{b}_{s1} & \boldsymbol{b}_{s1} & \boldsymbol{A}_s^2\boldsymbol{b}_{s2} + \boldsymbol{A}_s\boldsymbol{b}_{s2} + \boldsymbol{b}_{s2} \end{bmatrix} \cdots (49)$$
$$(\sigma_1, \sigma_2) = (4, 0)$$
$$\Rightarrow \boldsymbol{B} = \begin{bmatrix} \boldsymbol{A}_s^3\boldsymbol{b}_{s1} & \boldsymbol{A}_s^2\boldsymbol{b}_{s1} & \boldsymbol{A}_s\boldsymbol{b}_{s1} & \boldsymbol{b}_{s1} \end{bmatrix} \cdots\cdots\cdots\cdots (50)$$

The simulation result is shown in Fig. 7 and Fig. 8. From the simulation results, PTC cannot be achieved with the conventional method, but it can be achieved in all three cases of the proposed method. The effectiveness of the proposed method is verified.

4.3 Experiment Results In the experiment, the proposed method of $(\sigma_1, \sigma_2) = (2, 2)$, the conventional method 1, and the conventional method 2 are compared under the same conditions as the simulation.

The experiment result is shown in Fig. 9 and Fig. 10. From the experiment results, the tracking errors of the proposed method are the smallest compared with that of the conventional methods. The effectiveness of the proposed method is verified.

5. Conclusion

The 6 DOF high-precision stage has the coupling problem. In the conventional methods, the decoupling methods such as a precompensator are used, and the system is controlled as a SISO system. However, when the precompensator and SISO multirate feedforward controller are used, it is theoretically impossible to achieve PTC since the unstable zeros are generated by the discretization. In the proposed method, MIMO multirate feedforward controller achieves PTC. In this paper, the effectiveness of the proposed method is shown in the simulation and the experiment of controlling 2 DOF (x, θ_y) of the high-precision stage. The differences in the control performance depending on how to select generalized controllability indices are considered in future works.

The proposed method relaxes the restrictions of mechanical design to suppress interference problem, therefore, the freedom of mechanical design is improved.

References

(1) Butler, H.: Position Control in Lithographic Equipment [Applications of Control], *IEEE Control Systems*, Vol. 31, No. 5, pp. 28–47 (2011).

(2) Moore, G. E.: Cramming More Components Onto Integrated Circuits, *Electronics*, Vol. 38, No. 8 (1965).

(3) Ohnishi, W., Fujimoto, H., Sakata, K., Suzuki, K. and Saiki, K.: Integrated design of mechanism and control for high-precision stages by the interaction index in the Direct Nyquist Array method, in *2015 American Control Conference (ACC)*, pp. 2825–2830, IEEE (2015).

(4) Tomizuka, M.: Zero Phase Error Tracking Algorithm for Digital Control, *Journal of Dynamic Systems, Measurement, and Control*, Vol. 109, No. 1, p. 65 (1987).

(5) Chen, T. and Francis, B. A.: *Optimal Sampled-Data Control Systems*, Springer London, London, 411 pp. (1995).

(6) Fujimoto, H., Hori, Y. and Kawamura, A.: Perfect tracking control based on multirate feedforward control with generalized sampling periods, *IEEE Transactions on Industrial Electronics*, Vol. 48, No. 3, pp. 636–644 (2001).

(7) Fujimoto, H.: *General Framework of Multirate Sampling Control and Applications to Motion Control Systems*, PhD thesis (2000).

(8) Ohnishi, W., Fujimoto, H., Sakata, K., Suzuki, K. and Saiki, K.: Decoupling Control Method for High-Precision Stages using Multiple Actuators considering the Misalignment among the Actuation Point, Center of Gravity, and Center of Rotation, *IEEJ Journal of Industry Applications*, Vol. 5, No. 2, pp. 141–147 (2016).

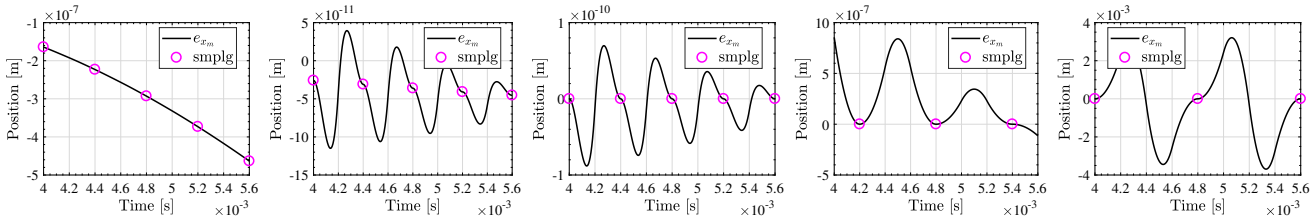

(a) Conventional method 1. (b) Conventional method 2. (c) Proposed method $(\sigma_1, \sigma_2) = (2, 2)$. (d) Proposed method $(\sigma_1, \sigma_2) = (3, 1)$. (e) Proposed method $(\sigma_1, \sigma_2) = (4, 0)$.

Fig. 7. Simulation result of e_{x_m} (zoom).

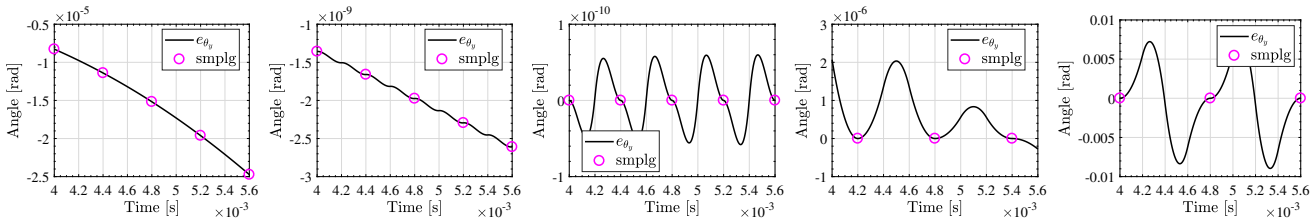

(a) Conventional method 1. (b) Conventional method 2. (c) Proposed method $(\sigma_1, \sigma_2) = (2, 2)$. (d) Proposed method $(\sigma_1, \sigma_2) = (3, 1)$. (e) Proposed method $(\sigma_1, \sigma_2) = (4, 0)$.

Fig. 8. Simulation result of e_{θ_y} (zoom).

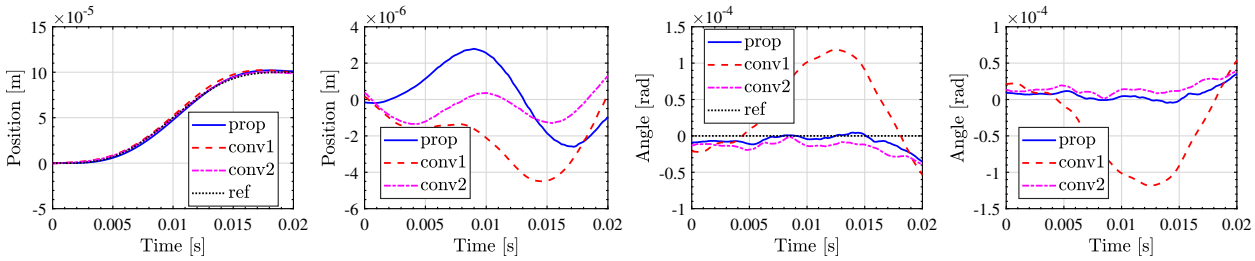

(a) x_m (b) e_{x_m} (c) θ_y (d) e_{θ_y}

Fig. 9. Outputs of the experimental results.

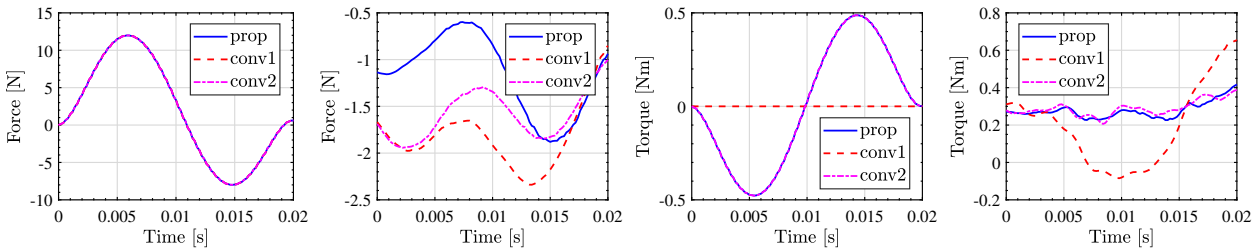

(a) $f_{x_{ff}}$ (b) $f_{x_{fb}}$ (c) $\tau_{y_{ff}}$ (d) $\tau_{y_{fb}}$

Fig. 10. Inputs of the experimental results.